Title
EXAFS Spectroscopy of Fractional Mixed-Valence Charge Density Wave Systems

Journal
The Journal of Physical Chemistry C, 123(10)

ISSN
1932-7447

Authors
Turner, NA
Kim, SS
Brozik, JA
et al.

Publication Date
2019-03-14

DOI
10.1021/acs.jpcc.8b12229

Peer reviewed

EXAFS Spectroscopy of Fractional Mixed-Valence Charge Density Wave Systems

N. A. Turner,[†] S. S. Kim,[‡] J. A. Brozik,[‡,§] M. A. Marcus,[∥] S. C. Fakra,[∥] and S. L. Dexheimer*[,†,‡]

[†]Department of Physics and Astronomy, [‡]Materials Science and Engineering Program, and [§]Department of Chemistry, Washington State University, Pullman, Washington 99164, United States

[∥]Advanced Light Source, Lawrence Berkeley National Laboratory, Berkeley, California 94720, United States

ABSTRACT: We present extended X-ray absorption fine structure (EXAFS) spectra and modeling of a series of structurally tunable quasi-one-dimensional mixed-valence platinum−halide linear chain materials, $[Pt(en_2)][Pt(en_2)X_2](ClO_4)_4$ with X = Cl, Br, I. The materials exhibit a commensurate charge density wave with fractional charge states on alternating platinum ions in the chain, as well as a Peierls distortion with alternating platinum−halide bond lengths. The amplitude of the charge density wave and, correspondingly, the extent of the Peierls distortion are controlled by the identity of the bridging halide ion. We have carried out ab initio multiple scattering calculations using the FEFF9 code to relate the oriented Pt L_{III} EXAFS spectra to the tunable electronic and structural properties. The spectral modeling reveals distinct photoelectron threshold energy values for the two inequivalent platinum ions in each of the mixed-valence chains, with values that vary systematically with fractional valence state. The difference in the photoelectron threshold energies of the two inequivalent platinum ions within each material correlates directly with the amplitude of the charge density wave, reflecting the decrease in charge density wave strength through the halide series X = Cl, Br, and I. We use dynamical matrix modeling to relate the experimentally determined mean-square relative displacement parameters for the metal−halide bond distances to the chain−axis vibrational modes that modulate the charge density wave structure. In addition, we discuss the EXAFS fitting results for the Pt−I bond lengths in the $[Pt(en_2)][Pt(en_2)I_2](ClO_4)_4$ complex in comparison to previous, mutually inconsistent structural determinations for this material.

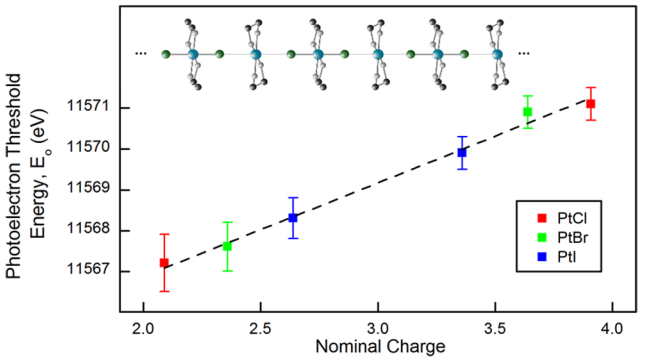

INTRODUCTION

Mixed-valence halide-bridged transition-metal linear chain (MX) complexes have proven to be excellent model systems for investigating a range of phenomena inherent to correlated electron systems owing to their structural tunability.[1−4] The properties of the materials are determined by competing electron−phonon and electron−electron interactions, which can be systematically tuned by varying the metal ion (M) and the halide ion (X) that comprise the linear chain structure. In the platinum−halide (PtX) materials studied here, the ground electronic state is a Peierls-distorted commensurate charge density wave (CDW). The relative strength of the electron−phonon coupling in the PtX materials can be tuned by the choice of the halide bridging ion X = Cl, Br, and I, resulting in a systematic variation of the strength of the Peierls distortion and of the amplitude of the CDW.

The structure of the representative $[Pt(en)_2][Pt(en)_2Cl_2]\cdot$ hybridization of the chain−axis orbitals to form two bands: a higher-energy, half-filled band of predominantly Pt $5d_z^2$ character and a lower-energy, fully filled band of predominantly halide p_z character. The Peierls distortion splits the half-filled $5d_z^2$ band to form valence and conduction bands and is accompanied by charge disproportionation, creating the CDW. The amplitude of the CDW has been characterized by a charge disproportionation parameter δ, such that Pt ions with a nominal formal valence of +3 disproportionate to give alternating $+(3 + \delta)$ and $+(3 - \delta)$ states. The limit $\delta = 0$ corresponds to a uniform valence state of Pt^{3+} for all sites, $\delta = 1$ corresponds to maximum charge transfer giving alternating Pt^{2+} and Pt^{4+} sites, and intermediate values correspond to fractional mixed valency. The fractional charge states of the platinum ions in the PtX complexes have been estimated by modeling[5] of X-ray photoelectron spectra (XPS),[6] using the formal valence states of monovalent monomeric subunits as reference standards. This modeling yields estimates of $\delta_{Cl} \sim$

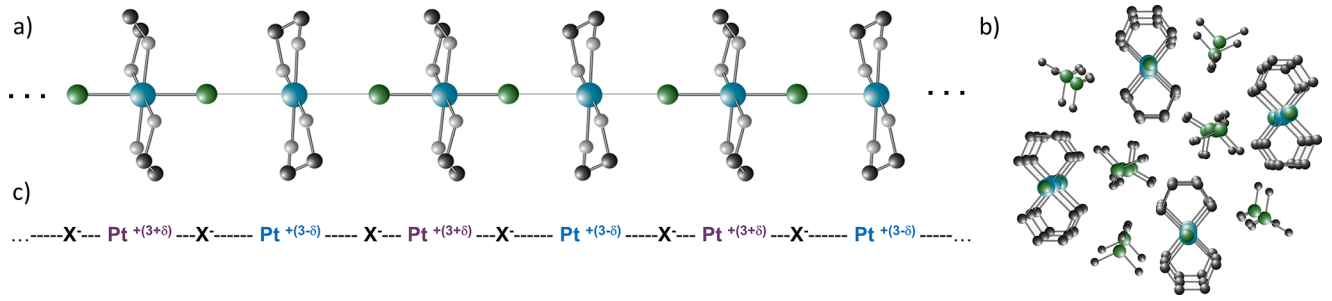

Figure 1. Structure of the $[Pt(en)_2][Pt(en)_2Cl_2]\cdot(ClO_4)_4$ (en = ethylenediamine) complex.[7] (a) Three repeat units of the $[Pt(en)_2][Pt(en)_2Cl_2]$ chain. (b) Crystal packing of the chains and ClO_4^- counterions, viewed down the chain axis. For clarity, only a short segment of the extended chain structure is presented and H atoms are omitted from the structures. (c) Schematic chain−axis structure with the amplitude of the charge density wave represented by the charge disproportionation parameter δ. (a) and (b) are reprinted with permission from ref 8, copyright 1999 American Physical Society; (c) is reprinted in part with permission from ref 4, copyright 2013 IOP Publishing.

0.91 for PtCl(en), $\delta_{Br} \sim 0.64$ for PtBr(en), and $\delta_I \sim 0.36$ for PtI(en), reflecting the systematic decrease in CDW amplitude through the halide series.

In the work presented here, we provide further characterization of the CDW properties of the PtX(en) materials using extended X-ray absorption fine structure (EXAFS). EXAFS provides information about the local structure around an absorbing atom, and also provides information about the electronic structure and the lattice dynamics through its dependence on the absorber photoelectron threshold energy and mean-square relative displacement (MSRD) parameters. In this work, we present modeling of EXAFS measurements carried out using the ab initio X-ray absorption code[9] FEFF9 together with multiparameter fitting. The results show systematic variation of the photoelectron threshold energy with the fractional mixed-valence state of the platinum ions, reflecting the tunable CDW amplitudes in the MX materials and demonstrating the ability of ab initio modeling of EXAFS spectra to extract valence state information in mixed-valence systems. The EXAFS fitting also yields values of the mean-square relative displacements of the platinum and halide ions, and we apply a dynamical matrix approach to relate the results to thermal population of chain−axis vibrational modes that modulate the CDW structure. The EXAFS studies on the PtI complex provide a point of comparison with previous structural determinations, providing additional evidence for polymorphism in this material. In addition to further characterizing the CDW properties, these results provide key parameters for modeling of other spectroscopies of the materials, and will provide the basis for further studies to probe their electronic excitations via the time-resolved X-ray absorption response.

METHODS

EXAFS measurements were performed at the Advanced Light Source microprobe beam line[10] 10.3.2 at the Pt L_{III} edge using a Si(111) double-crystal monochromator. The monochromator energy was calibrated using a Pt metal foil, with the Pt L_{III} edge set to 11 562.76 eV as determined by Kraft et al.[11] The intensity of the incident X-ray beam was monitored using an Ar-filled ionization chamber before the sample, and transmission and fluorescence measurements were carried out simultaneously. Fluorescence emission was collected using a seven-element Ge solid-state detector (Canberra, ON), while transmitted photons were detected using a second Ar-filled ionization chamber. Monochromator scans were carried out with increasing energy spacing to give a constant spacing in k-space of 0.05 Å^{-1} in the EXAFS region, and the integration time was increased throughout the k range to partially compensate for lower signal level with increasing energy.

The $[Pt(en_2)][Pt(en_2)X_2](ClO_4)_4$ (X = Cl, Br, I) complexes were synthesized using literature solution phase methods,[7,12] yielding single-crystal samples having a plate-like morphology with the chain axis lying in the plane of the plate. Measurements were carried out on oriented single crystals at near-normal incidence with the electric field of the incident polarized X-ray beam parallel to the chain axis as well as perpendicular to the chain axis in the plane of the plate. The samples were maintained at room temperature. Since these organometallic materials are susceptible to radiation damage, as evidenced by changes in white line and EXAFS features with continued exposure, care was taken to limit sample exposure so that signal changes were negligible within the collection time, and to this end, EXAFS scans were collected on multiple sample locations and averaged.

Initial data processing, including detector dead-time correction for fluorescence measurements, energy calibration, and glitch removal, was performed using custom LabVIEW software, and additional data reduction and analysis were performed using programs from the IFEFFIT (version 1.2.7) analysis package[13,14] together with FEFF9 (version 9.6 revision 4).[9] Scan merging, normalization, background removal, and Fourier transform windowing were carried out using Athena (version 0.8.057).[13] The photoelectron threshold energy E_o, the excitation energy at which the photoelectron is ejected into the continuum, enters through the conversion of data collected as a function of incident X-ray energy E to k-space using the relation

$$(E - E_o) = \frac{\hbar^2 k^2}{2m_e} \quad (1)$$

where k is the photoelectron wavevector. For the initial conversion of the data to k-space, E_o was set to the peak of the white line feature at 11566.7 eV, and E_o was later varied as a fitting parameter, as discussed below. Fluorescence data were corrected for over-absorption by matching the amplitude of the k-space data to the corresponding transmission data using the Tröger[15] method in Athena. The k-space data were windowed at zero crossings at low k (3.0 Å^{-1}) and at high k (11.5−14 Å^{-1}), depending on the signal shape and signal-to-noise ratio of each data set. The forward Fourier transformed R-space data were windowed (1−4.5 Å) to remove noise at low and high R.

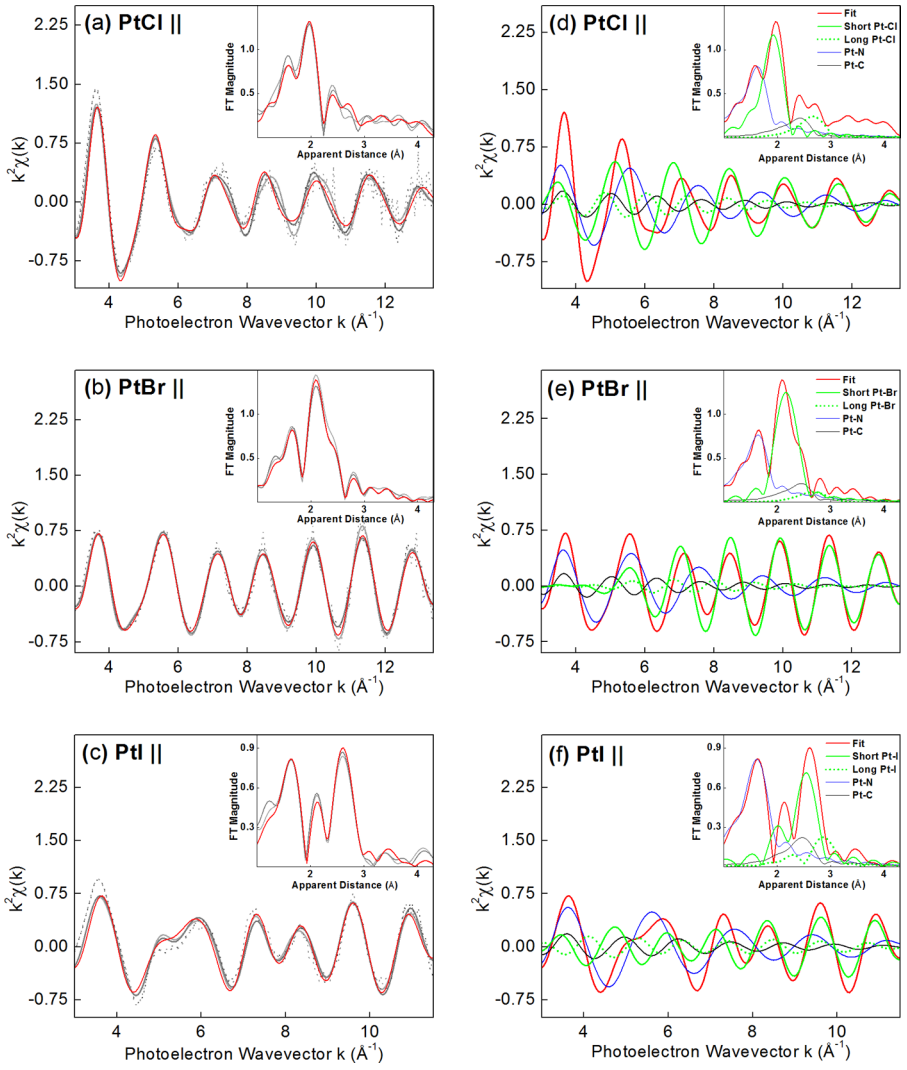

Figure 2. k^2-Weighted Pt L_{III}-edge EXAFS for X-ray polarization parallel to the chain axis for (a) PtCl, (b) PtBr, and (c) PtI. *k*-Space data are presented as dotted lines (transmission in dark gray and fluorescence in light gray), along with the back transformed Fourier-filtered response in solid gray and the corresponding fit in red. The fit is presented along with the signal components from single scattering paths in panels (d)−(f). Insets present the magnitude of the Fourier transform of the corresponding signals in *R*-space.

The forward Fourier transformed parallel and perpendicular oriented EXAFS spectra were fit simultaneously for each chain complex, and all spectra were fit simultaneously at *k*-weights of *k*, k^2, and k^3 to reduce correlations between fitting variables. The X-ray absorption near-edge structure (XANES) response, which is dominated by transitions to bound states, was analyzed with other techniques and will be reported separately.

Fitting of EXAFS spectra was performed using Artemis (version 0.08.012),[13] which uses the multiple-scattering path expansion of FEFF. In this approach, the EXAFS response is expressed as a sum of contributions from scattering paths of the photoelectron ejected from the absorbing atom

$$\chi(k) = S_o^2 \sum N_i \frac{f_{eff_i}(k)}{kr_i^2} e^{-2r_i/\lambda(k)} e^{-2k^2\sigma_i^2} \sin(2kr_i + \delta_i(k)) \quad (2)$$

Single-scattering (SS) paths, which involve backscattering of the photoelectron emanating from the absorber atom from a nearby atom, are characterized by an absorber−scatterer distance r_i, a scattering amplitude $f_i(k)$, a scattering phase shift $\delta_i(k)$, and the number of equivalent scatterers N_i. In the FEFF formalism, the expression generalizes to include multiple-scattering (MS) paths, which involve scattering of the photoelectron from two or more nearby atoms before returning to the absorbing atom, with the introduction of an effective scattering amplitude $f_{eff_i}(k)$, corresponding phase shift, and path degeneracy N_i. Each path is subject to two damping terms. The first takes into account inelastic scattering losses via a mean free path for the photoelectron, $\lambda(k)$. The second damping term accounts for static and thermal disorder as described by σ_i^2, the mean-square relative displacement (MSRD, also referred to as the EXAFS Debye−Waller factor) of the atoms involved in each scattering path. An overall amplitude factor S_o^2 accounts for many-body effects and, as a fitting parameter, may also correct for small variations in detected signal amplitude due to experimental conditions.

Given a model structure, FEFF enumerates the scattering paths and calculates $f_{eff_i}(k)$ and $\delta_i(k)$ for each path, along with $\lambda(k)$. These results are then used in Artemis to fit the data by varying parameters in eq 2. The structures of the PtX complexes have been determined previously by X-ray diffraction.[7,16−19] These crystallographic results were used in

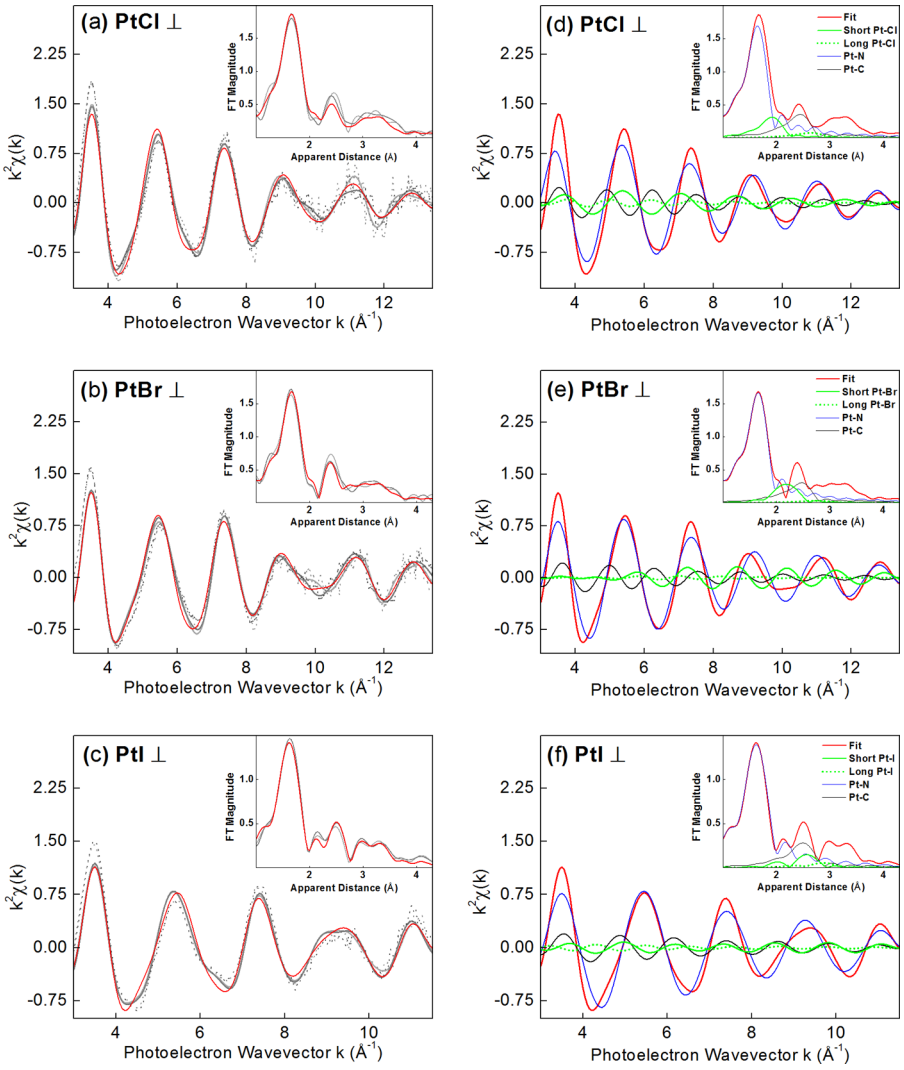

Figure 3. EXAFS responses for X-ray polarization perpendicular to the chain axis, presented as in Figure 2.

the Atoms program (version 0.9.25)[20] to generate the atomic positions that were input into FEFF9, where calculations of the scattering potentials were done using a self-consistent field (SCF) approach with Hedin–Lundqvist self-energy correction. By default, each element in a material is given a unique potential. For the mixed-valence materials studied here, additional potentials were assigned to provide unique potentials for each of the two inequivalent platinum ions in the chain structure and to provide two unique potentials for the nitrogen atoms that coordinate the two inequivalent platinum ions. In the case of the PtCl, the bridging chloride ion in the chain structure was given a different potential from that of the chloride ions in the perchlorate counterions. A separate set of paths was constructed for each of the two inequivalent platinum absorbers, and the resulting EXAFS response for each was weighted by a factor of 0.5 and summed for fitting to the experimental data.

Fitting of EXAFS data to eq 2 requires a choice of parameters to be varied in the fit, and a choice of scattering paths to be included in the fit. Four fitting parameters directly related to the CDW properties were allowed to vary: the photoelectron threshold energies of the two inequivalent platinum ions and the MSRDs for the SS paths for the two inequivalent platinum–halide distances along the chain axis. To reduce the number of variables in the fits, MSRDs for the Pt–N and Pt–C SS paths were fixed to the values reported by Provost et al.,[21] who determined EXAFS MSRDs for bis(ethylenediamine)platinate, which corresponds to the $Pt(en)_2$ subunit within the chain structure; allowing these values to vary yielded largely similar results. The MSRDs for MS paths were constructed from the SS MSRDs using geometric constraints. Distances were fixed using the structures determined by X-ray diffraction, with the exception of the Pt–I distances in the PtI complex, as discussed in the following section. The amplitude factor S_o^2 was allowed to vary independently for the parallel and perpendicular orientations and yielded values within the physically reasonable range of 0.85–1.05 for all data sets.

All single and multiple scattering paths with apparent distances $R < 4.5$ Å were included in the fits, with exceptions as noted. SS paths were included for the bridging halide ion and for the nitrogen and carbon atoms in the ethylenediamine ligands. Although the closest oxygen atom in the perchlorate counterion also fell within the $R = 4.5$ Å cutoff, it was not included, as it made a negligible contribution to the signal and accordingly yielded a large value with a large uncertainty for the MSRD associated with the scattering path, decreasing the quality of the fit. Although hydrogen atoms were included in

Table 1. Pt L_{III}-Edge EXAFS Curve Fitting Results[a]

complex	absorber	ΔE_o (eV)	Pt−X σ^2 ($\times 10^{-4}$ Å^2)	χ^2_v	R factor ($\times 10^{-3}$)	Pt−X bond length (Å)
PtCl				37.4	9.31	
	Pt(3 + δ_{Cl})	4.4(4)	26(3)			2.327*
	Pt(3 − δ_{Cl})	0.5(7)	115(25)			3.101*
PtBr				52.1	6.01	
	Pt(3 + δ_{Br})	4.2(4)	33(2)			2.484*
	Pt(3 − δ_{Br})	0.9(6)	160(28)			3.001*
PtI				43.7	8.12	
	Pt(3 + δ_I)	3.2(4)	49(4)			2.702(4)
	Pt(3 − δ_I)	1.6(5)	141(24)			3.05(2)

[a]*Pt−Cl and Pt−Br bond lengths were fixed to values determined by X-ray diffraction.[7] Pt−I bond lengths were allowed to vary as discussed in the text.

the ab initio calculations in FEFF9, scattering paths involving hydrogen atoms were not included in the fits. A number of MS paths involving atoms within the ethylenediamine ligands fell within the R = 4.5 Å cutoff. In addition, Pt−N−X triangle paths involving the shorter Pt−X distance fell within the cutoff for all three complexes, as well as that involving the longer Pt−I distance in the PtI complex. In the PtCl complex, the shorter Pt−Cl distance was sufficiently small to include Cl−Pt−Cl MS paths along the chain axis, as well as Pt−C−Cl paths involving the ethylenediamine ligands. Scattering paths with R > 4.5 Å were found to give a negligible contribution to the signal in all data sets.

RESULTS AND DISCUSSION

EXAFS measurements with polarization parallel to the chain axis together with fits to eq 2 are presented in Figure 2a−c for the three complexes, and the dominant signal components for each are presented in Figure 2d−f. The corresponding results for the perpendicular orientation are presented in Figure 3. As can be seen by comparing the two sets of measurements, the response is strongly dichroic, reflecting the highly anisotropic structure of the quasi-one-dimensional materials. L_{III}-edge transitions originate from 2p states and therefore include contributions from transitions to both s and d final states, with most of the signal due to p-to-d transitions, which are especially sensitive to anisotropy. For the parallel orientation, the dominant contribution to the EXAFS response is from backscattering from the halide ions at the shorter platinum−halide distance in the Peierls distorted chain structure, and the differences among the responses for the three complexes come primarily from the differing shape of $f(k)$ for the three halide ions. The dominant contribution to the perpendicular orientation EXAFS is from backscattering from the ethylenediamine nitrogen atoms, giving a similar response for all three complexes, as expected, given their similar transverse structure.

Photoelectron Threshold Energies. As can be seen from the fit results presented in Table 1, a distinct photoelectron threshold energy can be resolved for each of the two inequivalent platinum ions in each of the chain complexes. We note that the high precision of the photoelectron threshold energy values was made possible by inclusion of the MS paths in the fit, as the longer path lengths and therefore higher frequencies of these components in k-space makes them especially sensitive to E_o. The uncertainty in the E_o value for the platinum ion of higher charge is smaller than that for the ion of lower charge in each complex because the shorter halide distance gives stronger EXAFS components, allowing better determination of E_o. Figure 4 presents the resulting values for

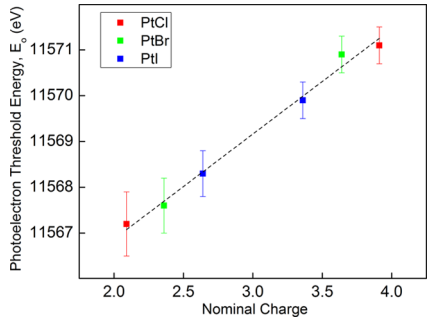

Figure 4. Fit results for the photoelectron threshold energy E_o of each of the two inequivalent platinum ions in the three mixed-valence complexes, plotted versus the nominal ion charge estimated from modeling[5] of XPS measurements,[6] showing the systematic variation with fractional valence state. The line is a linear fit to guide the eye. The difference between the E_o values for the two inequivalent platinum ions within each complex correlates with the charge density wave amplitude.

the photoelectron threshold energies, plotted as a function of the nominal platinum charge state estimated from modeling[5] of XPS measurements,[6] as described in the introduction. The photoelectron threshold energy is seen to increase systematically with valence, reflecting the higher electron binding energy with increasing fractional valence state as the nominal charge increases from +(3 − δ_{Cl}) = 2.09 for the platinum ion of lower charge in the PtCl complex to +(3 + δ_{Cl}) = 3.91 for the platinum ion of higher charge in the PtCl complex, with intermediate values in the PtBr and PtI complexes. The difference in photoelectron threshold energies for the two inequivalent platinum ions within each complex correlates directly with the amplitude of the CDW, decreasing systematically through the halide series X = Cl, Br, and I, reflecting the structural tunability of the materials. We note that the clear correlation between the photoelectron threshold energies and the nominal charge of the inequivalent platinum ions demonstrates the ability of ab initio modeling of EXAFS spectra to extract valence state information in mixed-valence systems. This approach may prove useful in other complex materials, in which traditional approaches such as XANES inflection energies can be problematic as a result of overlapping features from absorption edges of multiple valence states and from bound state transitions.

PtI Structure. Although the atomic positions determined by X-ray diffraction for the PtCl and PtBr complexes give an excellent match to the EXAFS spectra, none of the previously reported structures for the PtI complex give a good fit to the

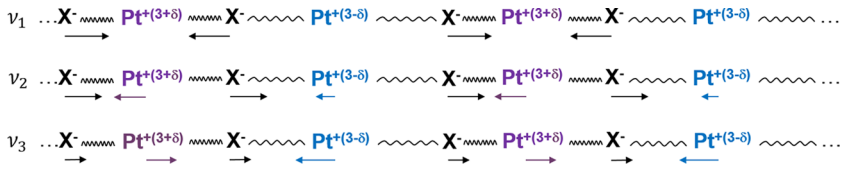

Figure 5. Chain−axis longitudinal optical phonon modes. Arrows represent atomic displacements as calculated for zone-center modes for PtCl. A longitudinal acoustic mode (not shown, as it has no zone center displacement) also contributes to the Pt−X mean-square relative displacements.

Table 2. Mean Square Relative Displacements for Pt−X Bonds with Phonon Mode Contributions Calculated Using the Dynamical Matrix Model of eq 3

	mean square relative displacement ($\times 10^{-4}$ Å^2)					
			dynamical matrix model mode contribution			
bond	experimental	dynamical matrix model	ν_1	ν_2	ν_3	acoustic
Pt(3 + δ_{Cl})−Cl	26(3)	27	12	13	1	1
Pt(3 − δ_{Cl})−Cl	115(25)	61	13	8	20	20
Pt(3 + δ_{Br})−Br	33(2)	32	13	15	3	1
Pt(3 − δ_{Br})−Br	160(28)	80	19	5	21	35
Pt(3 + δ_I)−I	49(4)	53	18	26	6	3
Pt(3 − δ_I)−I	141(24)	76	16	3	37	20

measured EXAFS response. A number of mutually inconsistent crystal structures have been reported for the PtI complex,[16−19] with significant discrepancies especially for the Pt−I distances. In general, structural determination of the PtX complexes by X-ray and neutron diffraction is complicated by the disorder inherent to the crystals, in which the phase of the CDW on adjacent chains is uncorrelated, as described, for example, in ref 7, and modeling of the structure from diffraction measurements can yield results that are dependent on the constraints imposed during the refinement procedure. In addition, for PtI, the structure has been seen to be sensitive to minor perturbations such as temperature, deuteration of the ethylenediamine ligands, and crystal growth conditions, and polymorphism has been reported,[19] likely accounting for a number of the discrepancies. In general, EXAFS provides a highly sensitive determination of distances between the absorbing atom and its nearby neighbors, independent of long-range crystalline order. Analysis of the EXAFS data for PtI was carried out using the atomic positions from the crystal structure reported by Endres et al.[16] as an initial model. In order to - obtain a good fit to the response, it was necessary to allow the Pt−I bond lengths to vary, as reported in Table 1. EXAFS fitting yields a decrease of 0.089(4) Å in the shorter Pt(3 + δ_I)−I bond length relative to the 2.791(8) Å reported by Endres et al., giving a value of 2.702(4) Å. The longer Pt(3 − δ_I)−I bond length is less well determined, as expected, given the smaller signal contribution from this component. EXAFS fitting yields a small increase of 0.01(2) Å, giving a value of 3.05(2) Å, which is within error of the value of 3.036(8) Å of Endres et al. The Pt−I bond lengths determined by EXAFS for the materials studied here lie within the range of those of the previously reported structures, which have short Pt−I bond lengths ranging between 2.677 and 2.791 Å and long Pt−I bond lengths ranging between 3.036 and 3.142 Å. Moreover, the ratio ρ of the short to long metal−halide bond lengths, a critical measure of the extent of the Peierls distortion in the CDW structure, also lies within the range of values for the previously reported structures: ρ = 0.886 for the EXAFS values reported here, compared to the range of 0.852−0.919 from the various diffraction studies. We note that the resolution of the EXAFS measurements is not sufficient to resolve four distinct Pt−I bond lengths, such as those reported in the structures of Matsumoto et al.[17] and Scott et al.;[19] however, the EXAFS spectra do not fit to the bond lengths reported for either of these structures.

Lattice Dynamics. The lattice dynamics of the PtX materials have attracted significant interest, in particular the low-frequency vibrational motions along the chain axis that modulate the CDW structure and also contribute to the structural relaxation that accompanies the formation of localized quasiparticles.[4,8,12,22] Here, we relate the Pt−X MSRDs determined by the EXAFS analysis to these vibrational modes. The structure along the chain axis, with two platinum and two halide ions in the Peierls-distorted repeat unit, yields four longitudinal modes: the three optical modes with the zone center displacements presented in Figure 5, along with an acoustic mode. The vibrational properties of the PtX materials have been investigated by Raman and IR spectroscopies[8,12,22−26] and have been modeled using dynamical matrix techniques.[22] The frequencies of the chain−axis vibrational modes lie in the range of ∼100−300 cm^{-1}, so they are substantially thermally populated at room temperature, where the EXAFS measurements were conducted.

The experimentally determined MSRDs for the Pt−X bonds are presented in Table 2, along with the results of dynamical matrix calculations that predict the contribution to the MSRDs from each of the four chain−axis vibrational modes. In these calculations, the dynamical matrix was constructed following the approach of Love et al.,[22] who modeled the vibrational properties of the PtX chains by including nearest and next-nearest neighbor harmonic contributions with force constants estimated from vibrational spectra. The matrix was constructed using a chain of 200 four-atom repeat units with periodic boundary conditions. The dynamical matrix was diagonalized to determine the normal-mode eigenvectors and eigenvalues, which yield the normalized displacements and frequencies for each phonon mode. These were used to calculate the MSRDs using the approach of Fornasini and Grisenti,[27] based on the formalism of Crozier.[28] For longitudinal motions along a one-dimensional axis, their expression for the MSRD reduces to

$$\sigma^2 \cong \frac{\hbar}{2\mu_{ab}} \times \sum_{q,s} \left| \left(\frac{\mu_{ab}}{m_b}\right)^{1/2} u_b(q, s) - \left(\frac{\mu_{ab}}{m_a}\right)^{1/2} u_a(q, s) \right|^2 \times \frac{1}{\omega(q, s)} \coth \frac{\hbar\omega(q, s)}{2k_bT} \quad (3)$$

where m_a, m_b, and μ_{ab} are the masses and reduced mass of the pair of atoms a and b, u_a and u_b are the normalized displacements for the atoms in the mode of wavevector q in phonon branch s, and ω is the mode frequency. For the PtX chains, m_a and m_b are the platinum and halide masses and u_a and u_b are the normalized displacements of those atoms for a given phonon mode. The sum in eq 3 is carried out over phonon wavevectors in the first Brillouin zone for the four longitudinal chain−axis phonon branches; the contributions from each of these branches are presented in Table 2.

As seen in Table 2, the dominant contributions to the MSRDs for the shorter Pt(3 + δ)−X bond in each complex come from the higher-frequency ν_1 symmetric stretch and ν_2 asymmetric stretch modes. The MSRDs for the longer Pt(3 − δ)−X bonds can be seen to include additional significant contributions from the lower-frequency ν_3 and acoustic modes. We find that the dynamical matrix model gives excellent agreement with the MSRD values for the shorter Pt−X bonds in each of the materials but underestimates the MSRDs for the longer Pt−X bonds. This likely results from limitations of the dynamical matrix modeling for the materials noted by Love et al., which overall have a larger effect on the lower-frequency modes. In particular, though the frequencies of the ν_1 and ν_2 modes are well-established by Raman and IR spectroscopy, the frequencies of the ν_3 modes have not been definitively established, and values for the next-nearest neighbor force constants could not be uniquely determined.[22] Since the lower-frequency ν_3 and acoustic modes are more dispersive than the higher-frequency ν_1 and ν_2 modes, and also have a larger thermal population, these uncertainties translate into larger discrepancies in the predictions for MSRDs dominated by the lower-frequency modes.

CONCLUSIONS

The EXAFS studies presented here provide further insight into the electronic structure of fractional mixed-valence materials. EXAFS fitting has yielded photoelectron threshold energies that reflect the variable charge on the platinum ions within the CDW materials. Comparison of the photoelectron threshold energies in the series of structurally tunable materials provides a new means to characterize their CDW states, as the difference in E_o values for the two inequivalent platinum ions in each material varies systematically with the degree of charge disproportionation. These results demonstrate the ability of ab initio modeling of EXAFS spectra to determine valence state information, an approach that may prove useful in other complex mixed-valence materials. Dynamical matrix modeling has also allowed us to relate the EXAFS MSRDs for the Pt−X bonds along the chain axis to the vibrational modes that modulate the CDW structure. Finally, comparison of EXAFS characterization of the Pt−I bond lengths in the PtI chain complex to the results of previous diffraction studies has provided further evidence of polymorphism in this material. The work presented here will inform further studies of the PtX materials and their excitations using X-ray spectroscopic techniques.

AUTHOR INFORMATION

Corresponding Author

*E-mail: dexheimer@wsu.edu. Phone: (509) 335-6389.

ORCID

J. A. Brozik: 0000-0003-2097-5051

S. L. Dexheimer: 0000-0003-2776-8792

Notes

The authors declare no competing financial interest.

ACKNOWLEDGMENTS

This work was supported by the National Science Foundation under awards DMR-1507538 and DMR-1106379. The Advanced Light Source is supported by the Director, Office of Science, Office of Basic Energy Sciences, of the U.S. Department of Energy under Contract No. DE-AC02-05CH11231. N.A.T. and S.L.D. thank John Rehr, Joshua Kas, and Fernando Vila for helpful discussions of the FEFF9 software package, and the authors thank Brian L. Scott for helpful discussions of X-ray diffraction studies of the materials.

REFERENCES

(1) Scott, B. L.; Love, S. P.; Kanner, G. S.; Johnson, S. R.; Wilkerson, M. P.; Berkey, M.; Swanson, B. I.; Saxena, A.; Huang, X. Z.; Bishop, A. R. Control of Selected Physical Properties of MX Solids: An Experimental and Theoretical Investigation. *J. Mol. Struct.* **1995**, *356*, 207−229.

(2) Gammel, J. T.; Saxena, A.; Batistić, I.; Bishop, A. R.; Phillpot, S. R. Two-Band Model for Halogen-Bridged Mixed-Valence Transition-Metal Complexes. I. Ground State and Excitation Spectrum. *Phys. Rev. B* **1992**, *45*, 6408−6434.

(3) *Material Designs and New Physical Properties in MX- and MMX-Chain Compounds*; Yamashita, M., Okamoto, H., Eds.; Springer-Verlag: Vienna, 2013.

(4) Morrissey, F. X.; Mance, J. G.; Van Pelt, A. D.; Dexheimer, S. L. Femtosecond Dynamics of Exciton Localization: Self-Trapping From the Small to the Large Polaron Limit. *J. Phys.: Condens. Matter* **2013**, *25*, 144204.

(5) Wada, Y.; Mitani, T.; Yamashita, M.; Koda, T. Charge-Transfer Exciton in Halogen-Bridged Mixed-Valent Pt-Complexes and Pd-Complexes - Analysis Based on the Peierls-Hubbard Model. *J. Phys. Soc. Jpn.* **1985**, *54*, 3143−3153.

(6) Yamashita, M.; Matsumoto, N.; Kida, S. Studies on Mixed-Valence Complexes of Platinum and Palladium. IV. X-ray Photoelectron Spectra of Some of the Platinum Complexes. *Inorg. Chim. Acta* **1978**, *31*, L381−L382.

(7) Huckett, S. C.; Scott, B. L.; Love, S. P.; Donohoe, R.; Burns, C. J.; Garcia, E.; Frankcom, T.; Swanson, B. I. Effects of Temperature on the Crystal and Molecular-Structure of the Mixed-Valence Linear-Chain $[Pt(en)_2][Pt(en)_2X_2](ClO_4)_4$ (X = Cl, Br). *Inorg. Chem.* **1993**, *32*, 2137−2144.

(8) Swanson, B. I.; Brozik, J. A.; Love, S. P.; Strouse, G. F.; Shreve, A. P.; Bishop, A. R.; Wang, W. Z.; Salkola, M. I. Observation of Intrinsically Localized Modes in a Discrete Low-Dimensional Material. *Phys. Rev. Lett.* **1999**, *82*, 3288−3291.

(9) Rehr, J. J.; Kas, J. J.; Vila, F. D.; Prange, M. P.; Jorissen, K. Parameter-Free Calculations of X-ray Spectra with FEFF9. *Phys. Chem. Chem. Phys.* **2010**, *12*, 5503−5513.

(10) Marcus, M. A.; MacDowell, A. A.; Celestre, R.; Manceau, A.; Miller, T.; Padmore, H. A.; Sublett, R. E. Beamline 10.3.2 at ALS: A Hard X-ray Microprobe for Environmental and Materials Sciences. *J. Synchrotron Radiat.* **2004**, *11*, 239−247.

(11) Kraft, S.; Stümpel, J.; Becker, P.; Kuetgens, U. High Resolution X-ray Absorption Spectroscopy with Absolute Energy Calibration for the Determination of Absorption Edge Energies. *Rev. Sci. Instrum.* **1996**, *67*, 681−687.

(12) Buschmann, W. E.; McGrane, S. D.; Shreve, A. P. Chemical Tuning of Nonlinearity Leading to Intrinsically Localized Modes in Halide-Bridged Mixed-Valence Platinum Materials. *J. Phys. Chem. A* **2003**, *107*, 8198−8207.
(13) Ravel, B.; Newville, M. ATHENA, ARTEMIS, HEPHAESTUS: Data Analysis for X-ray Absorption Spectroscopy Using IFEFFIT. *J. Synchrotron Radiat.* **2005**, *12*, 537−541.
(14) Newville, M. IFEFFIT: Interactive XAFS Analysis and FEFF Fitting. *J. Synchrotron Radiat.* **2001**, *8*, 322−324.
(15) Tröger, L.; Arvanitis, D.; Baberschke, K.; Michaelis, H.; Grimm, U.; Zschech, E. Full Correction of the Self-Absorption in Soft-Fluorescence Extended X-ray Absorption Fine Structure. *Phys. Rev. B* **1992**, *46*, 3283−3289.
(16) Endres, H.; Keller, H. J.; Martin, R.; Gung, H. N.; Traeger, J. The Structure of the Linear Chain Bis(1,2-diaminoethane)platinum-(II)bis(1,2-diaminoethane)diiodoplatinum(IV) Tetraperchlorate. *Acta Crystallogr. B* **1979**, *35*, 1885−1887.
(17) Matsumoto, N.; Yamashita, M.; Kida, S.; Ueda, I. Structure of a Pt^{II}−Pt^{IV} Mixed-Valence Complex, Bis(ethylenediamine)platinum-(II)-bis(ethylenediamine)diiodoplatinum(IV) Perchlorate, $[Pt(en)_2]$-$[Pt(en)_2I_2](ClO_4)_4$. *Acta Crystallogr. B* **1979**, *35*, 1458−1460.
(18) Bardeau, J. F.; Bulou, A.; Klooster, W. T.; Koetzle, T. F.; Johnson, S.; Scott, B.; Swanson, B. I.; Eckert, J. Neutron Diffraction Study of $[Pt(en)_2][Pt(en)_2I_2](ClO_4)_4$ at 20 K: Structure and Evidence of a New Phase Transition. *Acta Crystallogr. B* **1996**, *52*, 854−864.
(19) Scott, B. L.; Bracewell, B. L.; Johnson, S. R.; Swanson, B. I.; Bardeau, J. F.; Bulou, A.; Hennion, B. Synthesis and Characterization of a New Polymorph of PtI Containing an Ordered MX Chain. *Chem. Mater.* **1996**, *8*, 321−323.
(20) Ravel, B. ATOMS: Crystallography for the X-ray Absorption Spectroscopist. *J. Synchrotron Radiat.* **2001**, *8*, 314−316.
(21) Provost, K.; Beret, E. C.; Muller, D. B.; Michalowicz, A.; Sanchez Marcos, E. EXAFS Debye-Waller Factors Issued from Car-Parrinello Molecular Dynamics: Application to the Fit of Oxaliplatin and Derivatives. *J. Chem. Phys.* **2013**, *138*, No. 084303.
(22) Love, S. P.; Huckett, S. C.; Worl, L. A.; Frankcom, T. M.; Ekberg, S. A.; Swanson, B. I. Far-Infrared Spectroscopy of Halogen-Bridged Mixed-Valence Platinum-Chain Solids - Isotope-Substitution Studies. *Phys. Rev. B* **1993**, *47*, 11107−11123.
(23) Love, S. P.; Worl, L. A.; Donohoe, R. J.; Huckett, S. C.; Swanson, B. I. Origin of the Fine Structure in the Vibrational Spectrum of $[Pt(C_2H_8N_2)_2][Pt(C_2H_8N_2)_2Cl_2](ClO_4)_4$: Vibrational Localization in a Quasi-One-Dimensional System. *Phys. Rev. B* **1992**, *46*, 813−816.
(24) Degiorgi, L.; Wachter, P.; Haruki, M.; Kurita, S. Phonons in One-Dimensional Peierls-Hubbard Systems. *Phys. Rev. B* **1990**, *42*, 4341−4350.
(25) Degiorgi, L.; Wachter, P.; Haruki, M.; Kurita, S. Far-Infrared Optical Investigations on Quasi-One-Dimensional Halogen-Bridged Mixed-Valence Compounds. *Phys. Rev. B* **1989**, *40*, 3285−3293.
(26) Clark, R. J. H. Raman and Resonance Raman Spectroscopy of Linear Chain Complexes. In *Advances in Infrared and Raman Spectroscopy*; Clark, R. J. H., Hester, R. E., Eds.; John Wiley & Sons: New York, 1984; pp 95−132.
(27) Fornasini, P.; Grisenti, R. On EXAFS Debye-Waller Factor and Recent Advances. *J. Synchrotron Radiat.* **2015**, *22*, 1242−1257.
(28) Crozier, E. D.; Rehr, J. J.; Ingalls, R. Amorphous and Liquid Systems. In *X-ray Absorption: Principles, Applications, Techniques of EXAFS, SEXAFS, and XANES*; Koningsberger, D. C., Prins, R., Eds.; John Wiley & Sons: New York, 1988; pp 373−442.